OPEN ACCESS International Journal of Pharmacology

ISSN 1811-7775
DOI: 10.3923/ijp.2024.1112.1124

Research Article
Effect of Natural Extract Ligustrazine on the Proliferation of Laryngeal Squamous Cell Carcinoma Cells and its Impact on Ultrasound Imaging

[1]Kailan Xiao, [2]Yan Xiao and [2]Shuhua Liu

[1]Department of Ultrasound Diagnosis, Zhuzhou Hospital Affiliated to Xiangya School of Medicine, Central South University, Zhuzhou 412007, Hunan, China
[2]Department of Otolaryngology Head and Neck Surgery, Zhuzhou Hospital Affiliated to Xiangya School of Medicine, Central South University, Zhuzhou 412007, Hunan, China

Abstract

Background and Objective: Currently, our understanding of the specific mechanisms and effects of ligustrazine on laryngeal squamous cell carcinoma remains limited. This research evaluated the inhibition of ligustrazine on the proliferation of laryngeal squamous cell carcinoma (LSCC) cells and its impact on ultrasound imaging. The potential anti-tumor effect of ligustrazine and its influence on ultrasound imaging parameters were explored. **Materials and Methods:** Ligustrazine was extracted. The influence of ethanol concentration, volume, extraction frequency, duration and temperature on ligustrazine concentration was analyzed. The MTT assay evaluated ligustrazine's impact on cell proliferation capacity. Western blot assessed the expression of proteins related to the AKT/mTOR signaling. Twenty nude mice were divided into control and ligustrazine groups. Parameters of time-intensity curves were analyzed. **Results:** The highest extraction efficiency of ligustrazine was achieved by extracting it three times with 100 mL of 75% ethanol at 60°C for 180 min each time. The levels of p-AKT and p-mTOR proteins in LSCC cells were downregulated in the ligustrazine-treated groups ($p<0.05$). In the ligustrazine group, the tumor weight, tumor volume and parameters of contrast-enhanced ultrasound (acceleration time, ACT and increased signal intensity, ISI) were reduced ($p<0.01$). **Conclusion:** Ligustrazine regulates the proliferation capacity of LSCC cells through the AKT/mTOR SPW, promotes the dynamic response of blood flow, influences the dynamic behavior of blood flow and also influences the performance of contrast-enhanced ultrasound imaging.

Key words: Ligustrazine, LSCC, proliferation, signaling pathway, ultrasound imaging

Citation: Xiao, K., Y. Xiao and S. Liu, 2024. Effect of natural extract ligustrazine on the proliferation of laryngeal squamous cell carcinoma cells and its impact on ultrasound imaging. Int. J. Pharmacol., 20: 1112-1124.

Corresponding Author: Shuhua Liu, Department of Otolaryngology Head and Neck Surgery, Zhuzhou Hospital Affiliated to Xiangya School of Medicine, Central South University, Zhuzhou 412007, Hunan, China

Competing Interest: The authors have declared that no competing interest exists.

Data Availability: All relevant data are within the paper and its supporting information files.

INTRODUCTION

Laryngeal squamous cell carcinoma (LSCC) is malignant, which is derived from squamous epithelial cells and primarily occurs in the epithelial tissue of the laryngeal glottis but can also occur in other regions of the larynx[1]. Prolonged smoking, excessive alcohol consumption, chronic inflammation, viral infections, diabetes and genetic factors are associated with the development of LSCC[2,3]. These factors lead to genetic mutations, inactivation of tumor suppressor genes, activation of oncogenes, as well as abnormalities in apoptosis and cell cycle regulation within cellular signaling pathways (SPWs), ultimately resulting in cellular carcinogenesis and tumor growth[4]. Currently, LSCC in clinical practice can be treated by surgical resection, radiation therapy and chemotherapy. Chemotherapy is typically used for metastatic or advanced-stage patients, but it often faces challenges such as drug resistance, gastrointestinal reactions, bone marrow suppression and immunosuppression[5]. Therefore, finding a new method for treating LSCC holds significant importance.

Ligustrazine is an organic compound found in plants and is mainly extracted from *Ligusticum wallichii*. It has various effects[6-8]. Ligustrazine has been extensively studied and applied in the treatment of multiple diseases, particularly in cardiovascular and nervous system disorders, where it plays an important role[9]. Additionally, ligustrazine has shown potential in anti-tumor and immune modulation, attracting attention for its application in cancer treatment[10]. In the field of cancer therapy, ligustrazine has been investigated for various types of cancer[11,12]. Studies have demonstrated that ligustrazine can inhibit cancer cell proliferation, induce apoptosis and exhibit inhibitory effects on tumor angiogenesis and metastasis[13]. Ligustrazine can also enhance the efficacy of chemotherapy drugs and reduce their toxic side effects[14]. Mechanistic studies of ligustrazine suggest that its anti-tumor effects may be related to multiple signaling pathways involved in cell cycle regulation, apoptosis regulation, angiogenesis inhibition and immune modulation[15]. Ligustrazine can affect the expression of various target proteins and related genes[16,17]. Despite the potential demonstrated by ligustrazine in cancer treatment, its mechanisms of action and clinical applications are still under research. Moreover, its application in LSCC is limited and there is currently no research available regarding the effect of ligustrazine on LSCC cell proliferation.

Ultrasound imaging is a non-invasive and safe imaging technique that utilizes contrast agents to enhance the visualization of blood vessels and tissues[18]. This technology has been widely used in clinical diagnosis and treatment, particularly in tumor detection and evaluation. Ligustrazine, with its anti-inflammatory, anticoagulant and vasodilatory properties, has attracted attention for its potential application in ultrasound imaging. Previous studies have suggested that ligustrazine may have certain effects on ultrasound imaging[19]. However, the specific mechanisms and effects of ligustrazine on ultrasound imaging parameters are still not well understood. Further research is necessary to better understand the impact and potential applications of ligustrazine in ultrasound imaging.

Therefore, this work focused on the Hep-2 cell line of LSCC as the research target. Through laboratory cell culture and *in vitro* studies, it evaluated the inhibitory effect of ligustrazine on LSCC cell proliferation and explored its potential as an anti-tumor agent. The goal was to provide new therapeutic strategies and drug options for the treatment of LSCC. Additionally, this work utilized BALB/cA nu/nu mice as the animal model to analyze the therapeutic effect of ligustrazine on LSCC. Meanwhile, it assessed the impact of ligustrazine on parameters such as acceleration time (ACT), increased signal intensity (ISI), area under the curve (AUC) and blood flow coefficient (BF) to understand the potential application value of ligustrazine in ultrasound imaging. The findings intended to yield a scientific basis for the rational use of ligustrazine in clinical treatment.

MATERIALS AND METHODS

Study area: The research was performed in Zhuzhou Hospital Affiliated with Xiangya School of Medicine from December, 2021 to April, 2023.

Extracting and separating the natural extract ligustrazine: A certain amount of *Ligusticum wallichii* (Anhui Jinfurong Traditional Chinese Medicine Pieces Co., Ltd., China) was weighed and pulverized using a grinder, sieved through an 80-mesh sieve and accurately weighed at 6.0 g. It was then dissolved in 50 mL of anhydrous ethanol (China National Pharmaceutical Group Chemical Reagent Co., Ltd., China). The reflux extraction was performed using ethanol at different concentrations and extraction temperatures of 30, 40, 50, 60, 70, 80, 90 and 100°C. The extraction solution was filtered, vacuum-concentrated to dryness, added with an appropriate amount of water, heated to dissolve and filtered again. The filtrate was returned to a prepared macroporous resin column. The sample was added one drop every 3 seconds. After complete addition, the column was washed with water until the reducing sugar test showed a negative reaction. Then, 2-3 drops of 0.5% resorcinol solution were added and a slow

addition of 0.5 mL of concentrated sulfuric acid was performed. If a brown ring formed at the reaction site, it indicated a negative result. Elution with 30% ethanol until colorless was performed and the eluate was collected. After vacuum evaporation of ethanol and cooling, extraction with ethyl ether was carried out. The ethyl ether extract was subjected to extraction with 1 M concentrated sulfuric acid (Beijing Chemical Factory, China) and the acidic solution was alkalized with saturated sodium carbonate solution (Beijing Chemical Factory, China) solution to reach a pH of 9-10. Finally, extraction with chloroform was performed, followed by vacuum evaporation of chloroform to dryness, resulting in the total alkaloids from *Ligusticum wallichii*. The petroleum ether-soluble fraction of the total alkaloids was taken and petroleum ether was evaporated under reduced pressure, yielding an orange-yellow paste. This substance was placed on an alkaline Al_2O_3 column for chromatographic separation and eluted with a mixture of petroleum ether (China National Pharmaceutical Group Chemical Reagent Co., Ltd., China) and chloroform (China National Pharmaceutical Group Chemical Reagent Co., Ltd., China) (8:2). After vacuum concentration, the obtained product was subjected to sublimation crystallization, resulting in colorless needle-like crystals, which are ligustrazine. The specific processes of ligustrazine extraction, separation and purification were summarized in Fig. 1.

Analyzing the performance of ligustrazine: The ligustrazine content was determined by using the following operations. A small amount of 0.5% hydrochloric acid was mixed with a 5 mg sample of ligustrazine. The sample was heated to 70°C and continuously heated for 20 min. After cooling, the sample was made up to volume in a 10 mL volumetric flask, shaken well and centrifuged for 5 min using a centrifuge. Then, 2 mL of the sample was taken and made up to volume with 0.1 mol/L hydrochloric acid. The OD value of the sample was measured by a UV-visible spectrophotometer and the ligustrazine concentration was calculated.

A 5 mg sample of ligustrazine was weighed and added to a 20 mL solution of 0.1 mol/L hydrochloric acid, dissolved under 42°C conditions and transferred to a 25 mL volumetric flask, followed by dilution with 0.1 mol/L hydrochloric acid solution to the mark. The prepared solutions were then kept at room temperature (RT) and 4°C, respectively. Every 24 hrs, the OD value of ultraviolet-visible spectrophotometer (Beijing Optical Instrument Factory, China) at 298 nm was determined to analyze the stability.

Culture and grouping of cells: The LSCC cells were collected from patients diagnosed with LSCC. After surgical resection, the tissue was preserved and LSCC cells were isolated and cultured using an enzymatic digestion method. The primary LSCC cells were cultured in RPMI1640 medium (Invitrogen, USA) with 10% fetal bovine serum (Gibco, USA) at 37°C and 5% CO_2 in a temperature-controlled CO_2 cell culture incubator (Thermo Scientific, USA). Cell passaging was performed every 2 days to obtain LSCC cells in the logarithmic growth phase for later use. The LSCC cells were divided into different groups based on the concentration of the treatment drug and they were treated with ligustrazine at varying concentrations (0, 100, 200, 400, 600 and 800 mg/L).

Ethical consideration: This study was approved by the Ethics Committee of Zhuzhou Hospital Affiliated to Xiangya School of Medicine. The research objects were informed and they signed a fully informed consent form.

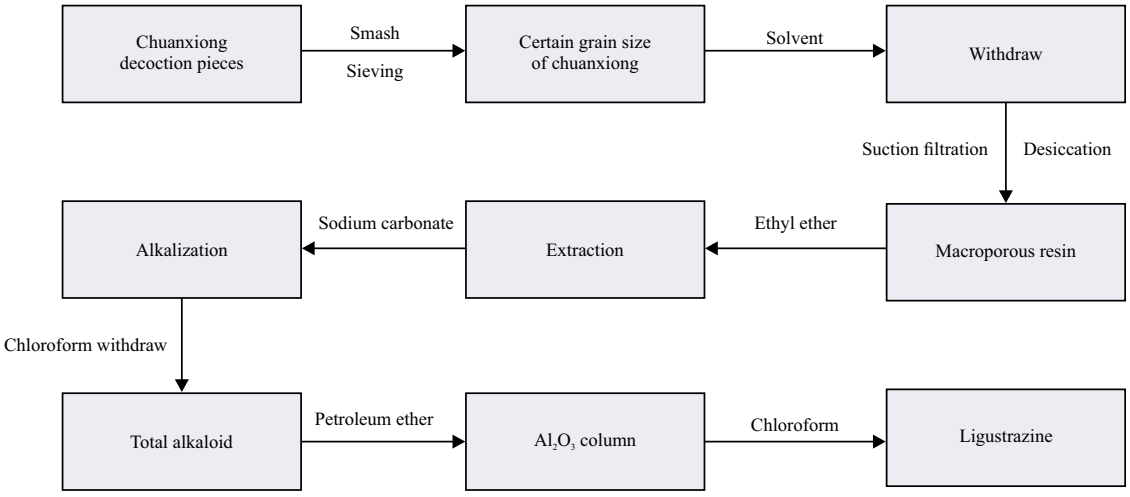

Fig. 1: Specific processes of extraction, separation and purification of ligustrazine

Impacts of ligustrazine on proliferation: The LSCC cells were rapidly revived and seeded in RPMI-1640 with 10% FBS and placed in an incubator with 5% CO_2 and a saturated humidity at 37°C. After reaching a confluence of around 90%, the cells were digested with 0.25% trypsin (Gibco, USA) and passaged at 4:1. Cells from the 3rd to 5th passage were used for subsequent experiments. The cell density was adjusted to 1×10^5 cells/mL and 100 µL of cell suspension was seeded in a 96-well plate for overnight incubation. The LSCC cells were then treated with different concentrations of ligustrazine. After 72 hrs of incubation, 10 µL of 5 mg/mL tetramethylrhodamine solution (Sigma-Aldrich, USA) was added to each well and incubated at 37°C for 4 hrs. Following that, 100 µL of 10% SDS containing 0.01 N HCl reagent was mixed to dissolve the formazan crystals. The OD value was examined at 570 nm. This process was repeated three times and cell proliferation inhibition rate (IR) was computed to be the percentage relative to the control group.

Western blot: The LSCC cell density was controlled at 1×10^5 cells/mL and 100 µL of the cell suspension was seeded for overnight incubation. After 24 hrs, the cells were grouped and treated accordingly. They were further incubated for 72 hrs and then the cells were collected. Total protein extraction was implemented using RIPA and the protein concentration was determined using a BCA kit. The total proteins were separated by 10% SDS-PAGE and then transferred onto a membrane. The membrane was blocked with 5% BSA for 1 hr. Primary antibodies against AKT (1:5000), p-AKT (1:5000), mTOR (1:5000), p-mTOR (1:5000) and β-actin (1:10000) were placed on the membrane and incubated all night at 4°C. Following a membrane washing with TBST, diluted secondary antibodies were added for incubation on a shaker at RT for 1 hr. Following another TBST treatment, the membrane was subjected to electrochemiluminescence detection according to the instructions of the detection kit. The protein bands were visualized using a gel imaging system and ImageJ software was utilized for statistical analysis of the relative grayscale values of the protein bands, with β-actin serving as an internal reference.

Establishment of LSCC animal models and grouping: Twenty BALB/cA nu/nu nude mice (8 weeks old, weighing 18 g; Shanghai Xipuer Bikai Experimental Animal Co., Ltd., China) were selected. The LSCC cell suspension (0.2 mL per mouse, containing 8.7×10^6 cells) was injected into the dorsal region of each mouse subcutaneously. Absorption of the injected fluid, tumor growth process and the condition of the mice were observed. After approximately 20 days, as long as the tumor volume exceeded 100 mm^3, the mice were rolled into different groups for further experiments. The research proceeded in compliance with the Ethics Guidelines of Animal Farewell and Care.

Randomly, the 20 nude mice were grouped into the control group and ligustrazine group, with 10 mice in each. In the ligustrazine group, a subcutaneous injection of ligustrazine at 50 mg/kg was administered, with an injection site located 3 mm away from the tumor edge. The Ctrl group received an equal volume of PBS solution. The administration was conducted for 10 days. The mice were weighed every 3 days. After a one-week drug withdrawal period, the mice were euthanized to dissect and weigh the tumors.

Ultrasound imaging on LSCC animal model: Three days after the establishment of the LSCC model, ultrasound imaging examinations were conducted on the nude mice. The examinations were performed every 3 days. Routine two-dimensional grayscale ultrasound and power Doppler imaging were performed using an L17-5 broadband linear array transducer. The routine two-dimensional grayscale ultrasound measured the three maximum perpendicular diameters of the subcutaneous tumor in the nude mice and calculated the tumor volume. The power Doppler imaging used a pulse repetition frequency of 250 Hz, wall filtering at 23 Hz and a color gain of 89%. During the examination, efforts were made to minimize motion artifacts by keeping the transducer as stable as possible. The blood flow signals within the tumor were recorded before and 2 min after the application of the contrast agent. Ultrasound imaging was performed using an L9-3 broadband linear array transducer, with a mechanical index (MI) of 0.1, a total gain of 95% and the focal point positioned below the tumor. All other settings remained consistent. The equation for calculating the tumor volume was as follows[20]:

$$V = T_d \times L_a \times A$$

where, V referred to the tumor volume and denoted the transverse and longitudinal diameter, respectively and represented the height.

The nude mice were intraperitoneally injected with 2.5 mg/kg pentobarbital for anesthetization. They were positioned in a lateral decubitus position on the operating table and a 5 mm thick layer of centrifugal coupling agent was applied to the transducer surface in contact with the tumor. For contrast-enhanced imaging, 20 µL of SonoVue was applied through the tail vein, followed by a flush of 0.2 mL of normal saline solution. The timing and image acquisition were started

immediately. Image acquisition was performed at a frame rate of 18 Hz and dynamic images were continuously acquired for 2 min. The acquired images were transferred to the SWtech Pacs workstation for offline analysis. The entire tumor and the central region 2-3 mm away from the tumor boundary were selected as regions of interest (ROI) to obtain the raw time-intensity curve (TIC) of the ROI. The parameters of the fitted TIC were analyzed using the least squares method to obtain the parameters of interest. These parameters included ISI, AUC, ACT and BF.

Statistical methods: Statistical analysis was implemented using SPSS 19.0. Data were presented as $\bar{\chi}\pm s$, where, $\bar{\chi}$ represented the mean value of the data set. The t-test and one-way analysis of variance were employed for analyzing the differences between two groups and among multiple groups, respectively. The $p<0.05$ was considered statistically significant.

RESULTS

Impacts from concentration and volume of ethanol on ligustrazine concentration: Variable concentrations of ethanol solutions (55, 65, 70, 75, 80, 85, 90 and 95%) were employed to extract ligustrazine. The changes in ligustrazine concentration after extraction with different ethanol concentrations were illustrated in Fig. 2a. As the ethanol solution concentration increased, the concentration of extracted ligustrazine initially increased and then decreased. The maximum concentration of ligustrazine (1.9123 μg/mL) was achieved when the ethanol solution concentration was 75%.

The impacts of different ethanol volumes (80, 90, 100, 110, 120, 130, 140, and 150 mL) on the extraction of ligustrazine concentration were analyzed, as demonstrated in Fig. 2b. As the ethanol volume increased, the concentration of extracted ligustrazine initially increased and then reached a stable level. When the ethanol volume was 100 mL, the concentration of extracted ligustrazine was 5.6802 μg/mL. However, beyond 100 mL, increasing the ethanol volume did not result in a further increase in ligustrazine concentration.

Influence of extraction cycles, time and temperature on ligustrazine concentration: The statistical results of the impact of extraction cycles on ligustrazine concentration were elaborated in Fig. 3a. As the extraction cycles increased, the extracted ligustrazine initially exhibited increased concentration and then a stable concentration. After 3 extraction cycles, the concentration of extracted ligustrazine was 5.8992 μg/mL. However, after more than 3 extraction cycles, increasing the extraction cycles did not further increase the concentration of ligustrazine.

Figure 3b demonstrated the statistical results of the impact of extraction time on ligustrazine concentration. As the extraction time increased, the concentration of extracted ligustrazine initially increased and then reached a stable level. When the extraction time was 180 min, the concentration of extracted ligustrazine was 8.6744 μg/mL. However, after exceeding 180 min of extraction time, extending the extraction time did not further increase the concentration of ligustrazine.

The impacts of extraction temperature on ligustrazine concentration were illustrated in Fig. 3c. With the extraction temperature increased, the concentration of extracted ligustrazine exhibited an increased trend initially but then decreased. At an extraction temperature of 60°C, the concentration of extracted ligustrazine was 4.5789 μg/mL, which was confirmed to be the maximal level. However, as the extraction temperature exceeded 60°C, the concentration of ligustrazine gradually decreased.

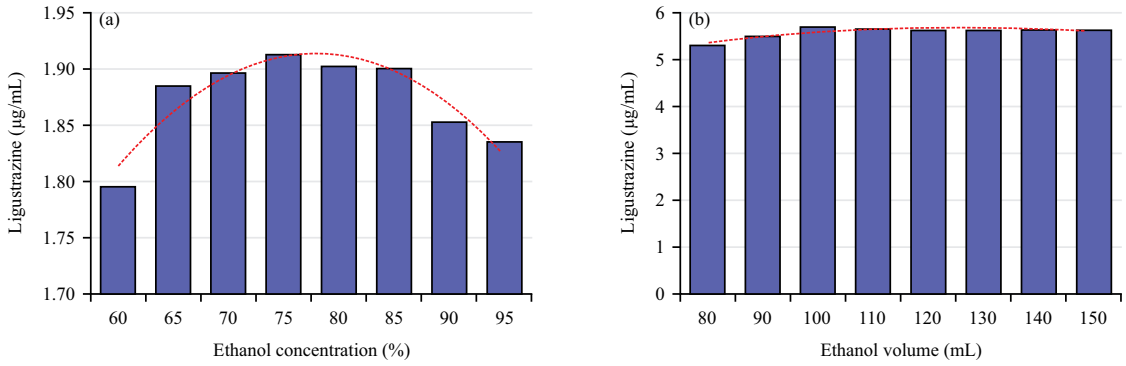

Fig. 2(a-b): Impacts from concentration and volume of ethanol on ligustrazine concentration

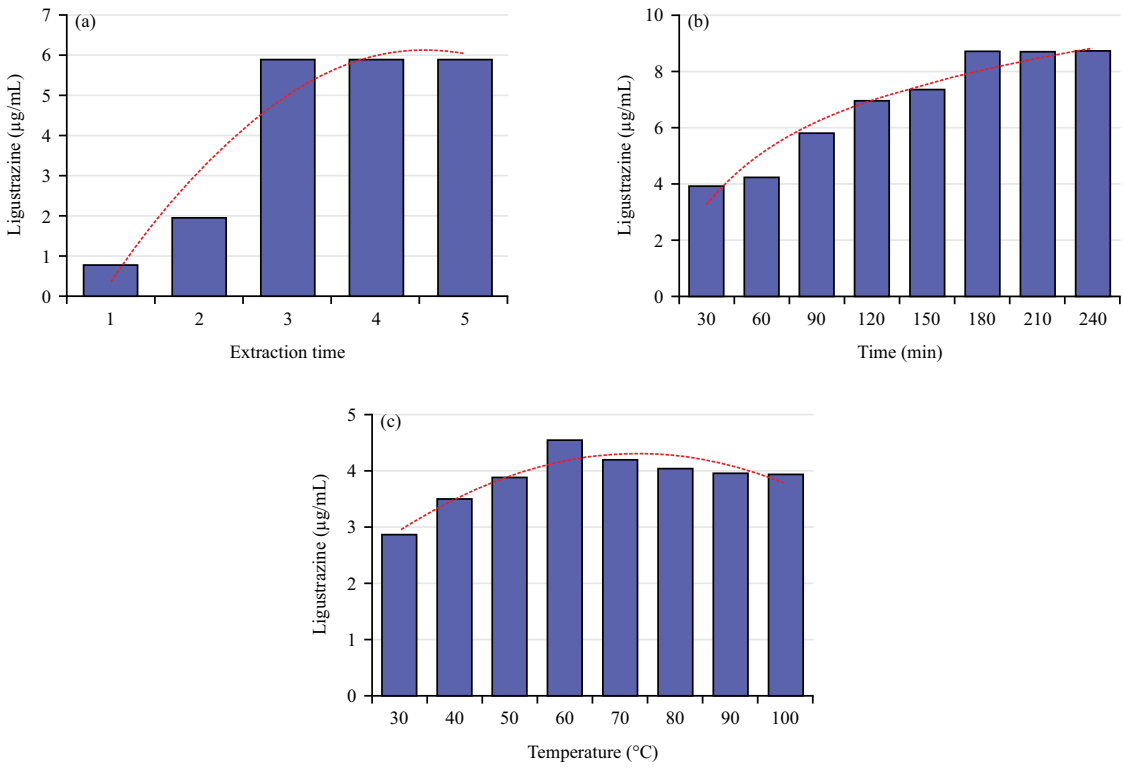

Fig. 3(a-c): Influence of extraction cycles, time and temperature on ligustrazine concentration

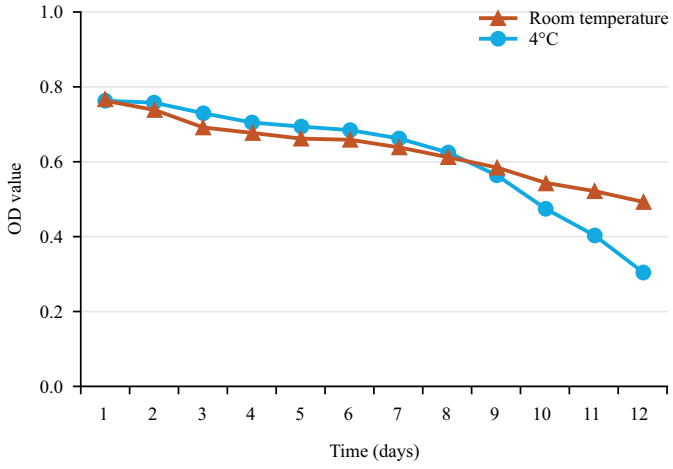

Fig. 4: Stability of ligustrazine

Stability of ligustrazine: The stability of ligustrazine was investigated under RT and 4°C conditions, as analyzed in Fig. 4. As time increased, OD values of ligustrazine decreased under both RT and 4°C conditions, with a slower decrease observed at 4°C.

Impacts of ligustrazine on proliferation of LSCC cells: Impacts of ligustrazine on proliferation ability of LSCC cells were displayed in Fig. 5. With increasing treatment time, IRs of LSCC cells treated with ligustrazine at 100, 200, 400, 600 and 800 mg/L all exhibited a great upward trend and were sharply different from the 0 mg/L group for the 100 and 200 mg/L ligustrazine treatments after 24 hrs ($p<0.01$). Meanwhile, those treated with 400, 600 and 800 mg/L ligustrazine were much higher to those in the 0 mg/L group at different time points, showing obvious differences ($p<0.001$).

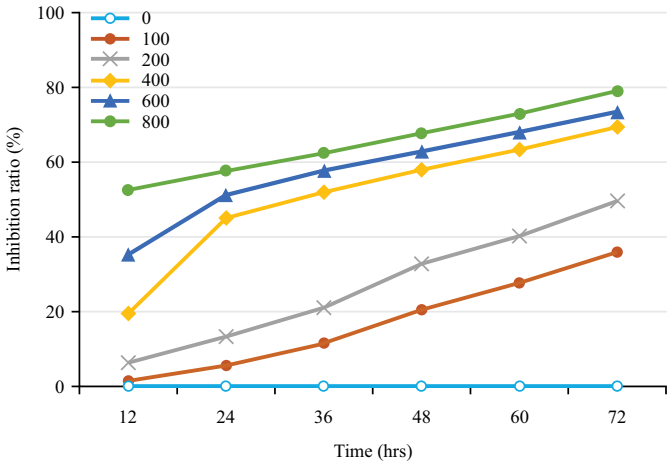

Fig. 5: Impacts of ligustrazine on proliferation of LSCC cells

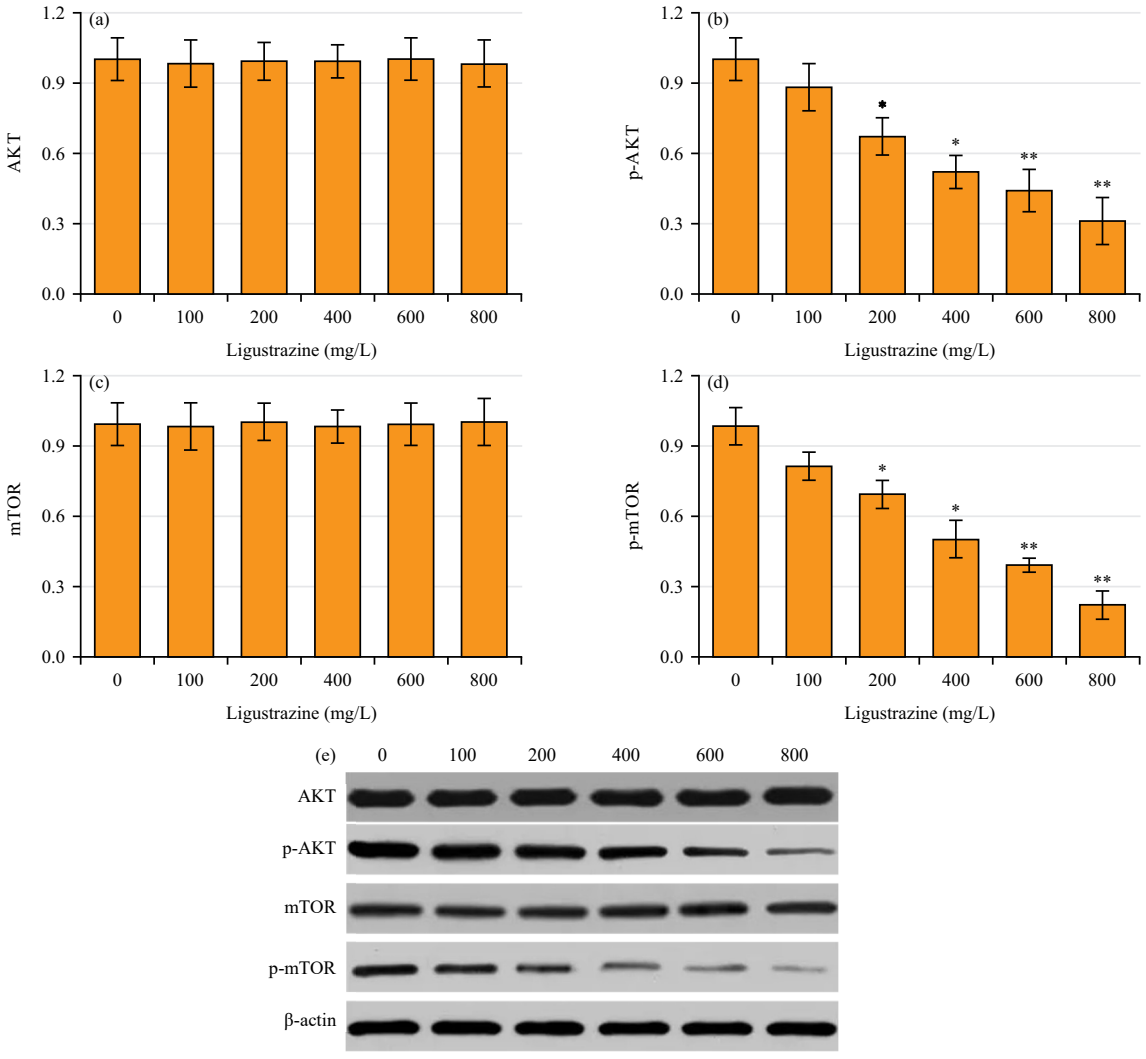

Fig. 6(a-e): Effects of ligustrazine on expressions of proteins related to the AKT/mTOR SPW, (a) AKT, (b) p-AKT, (c) mTOR, (d) p-mTOR and (e) Western blot results

*,**Suggested a great difference with $p<0.05$ and $p<0.01$, respectively

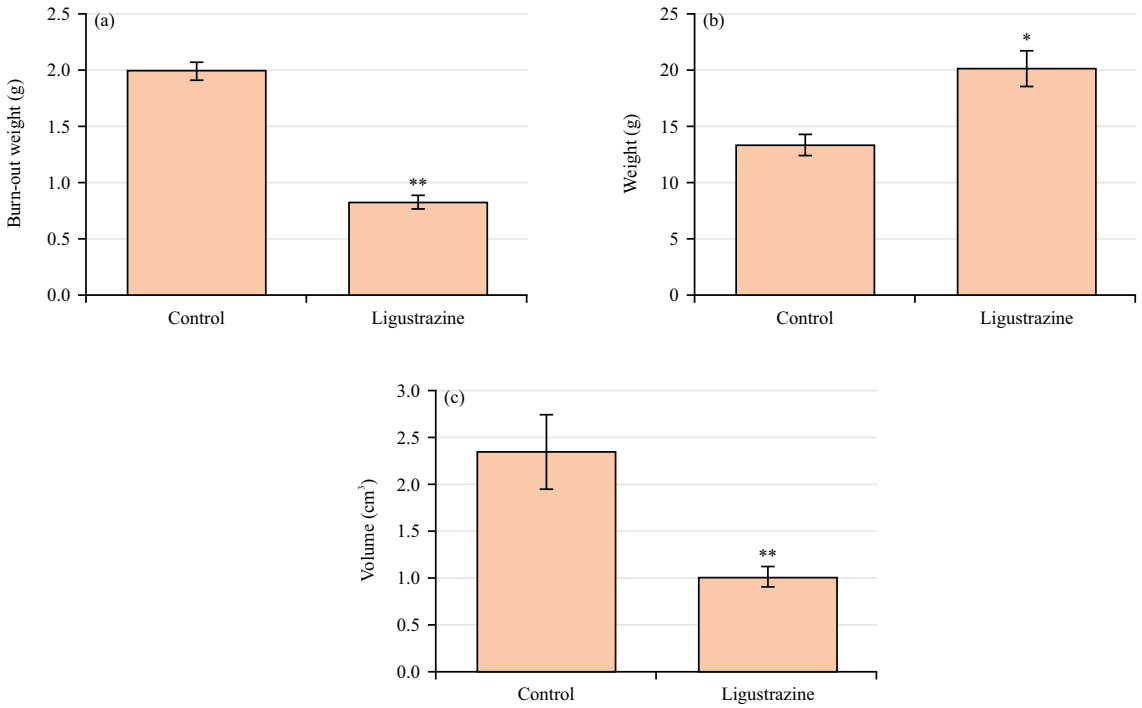

Fig. 7(a-c): Impacts of ligustrazine on tumor weight, net weight of mice and tumor volume in the LSCC model, (a) Tumor weight, (b) Net weight of mice and (c) Tumor volume

*,**Suggested a great difference with $p<0.05$ and $p<0.01$, respectively

Effects of ligustrazine on AKT/mTOR SPW: Changes in AKT, p-AKT, mTOR and p-mTOR in LSCC cells were compared in Fig. 6. No visible differences were observed in levels of AKT and mTOR between LSCC cells treated with 100, 200, 400, 600 and 800 mg/L of ligustrazine and those in the 0 mg/L group ($p>0.05$) (Fig. 6a, c and e). In contrast, with increasing concentrations of ligustrazine, p-AKT and p-mTOR showed a decreasing trend (Fig. 6b, d and e). Specifically, they were sharply lower in LSCC cells after treatment with 200 and 400 mg/L of ligustrazine, presenting great differences with $p<0.05$, but were obviously lower in 600 an d 800 mg/L of ligustrazine treatment groups ($p<0.01$).

Impacts of ligustrazine on tumor growth of LSCC model of nude mice: After modeling, all 20 nude mice were successfully inoculated and subcutaneous tumor formation was visible after about one week, which continued to grow with time. In the Ctrl group, the tumors were observed to increase in size as time went on and the nude mice showed poor physical condition and gradual weight loss. In the ligustrazine group, the nude mice were in good condition and the tumor growth was relatively slow with time and the change in body weight was not remarkable. Meanwhile, there were no deaths observed in either group during the intervention period.

The effects of ligustrazine on tumor weight, body weight and tumor volume in the LSCC model nude mice were summarized in Fig. 7. The tumor weight in the ligustrazine group was much lower, with a visible difference to the Ctrl group ($p<0.01$) (Fig. 7a). Body weight of mice in the ligustrazine group was higher, presenting a difference with $p<0.05$ to that in the Ctrl group (Fig. 7b). The tumor volume of mice in the ligustrazine group was lower, presenting an extremely considerable difference to that in the Ctrl group ($p<0.01$) (Fig. 7c).

The impacts of ligustrazine on tumor growth in different time periods were also analyzed (Fig. 8). With the extension of the intervention time, the tumor volume of nude mice in the ligustrazine group presented a stable trend, while the tumor volume in the Ctrl group showed an observable increase. Within the range of 3-9 days after intervention, the tumor volume in the ligustrazine group of nude mice was lower, exhibiting a statistical difference with $p<0.05$ to that in the Ctrl group. Within the range of 12-18 days after intervention, the tumor volume in the ligustrazine group of nude mice was sharply lower in comparison to the condition in the Ctrl group ($p<0.01$).

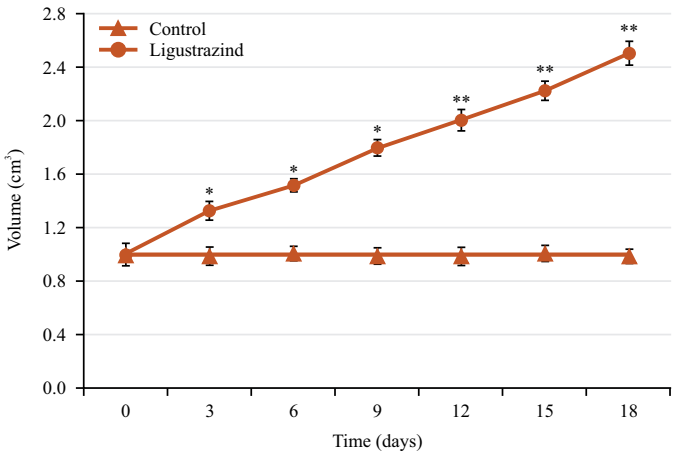

Fig. 8: Impacts of ligustrazine on tumor volume of nude mice with LSCC at different time intervals
*,**Suggested a great difference with p<0.05 and p<0.01, respectively

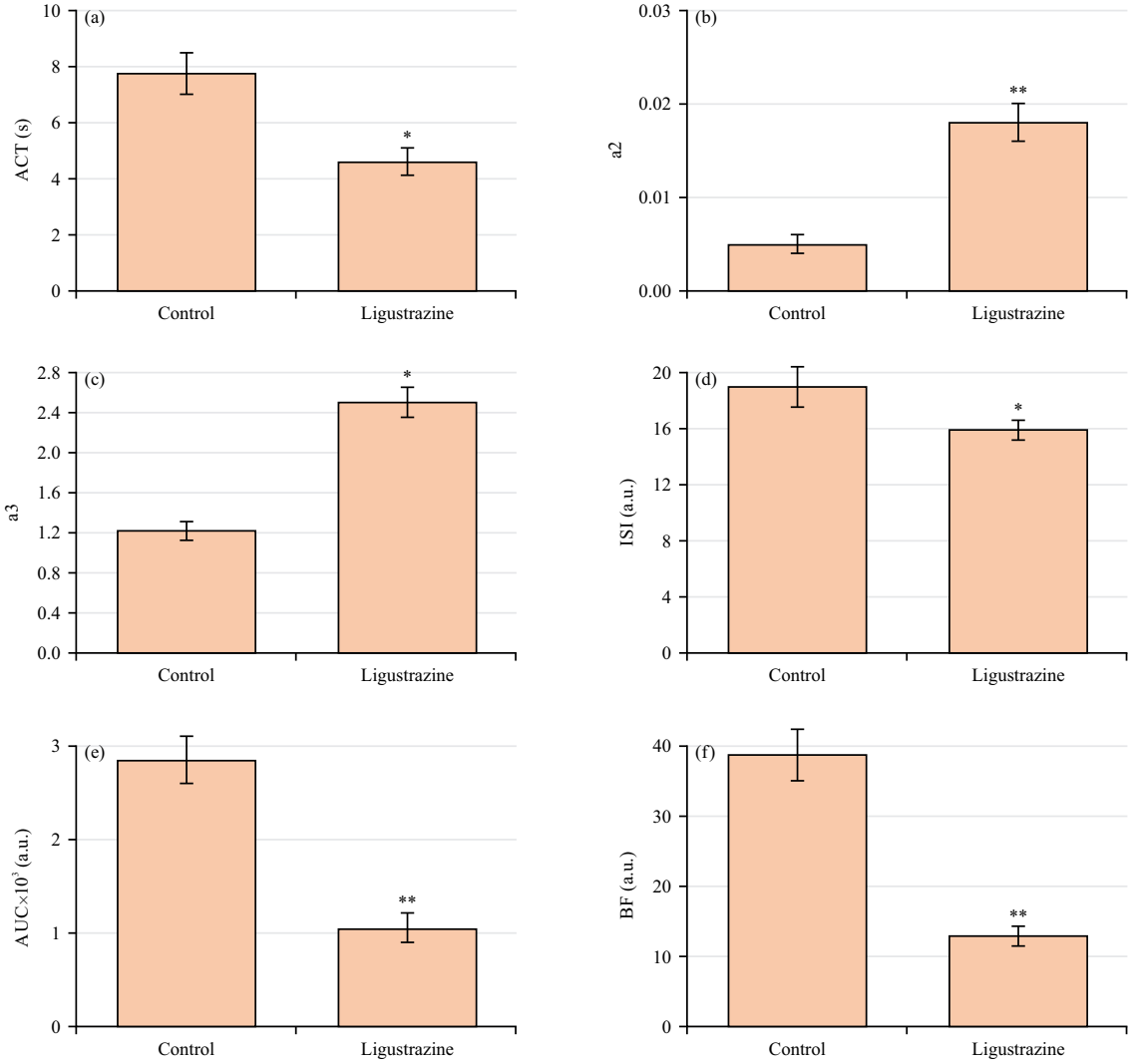

Fig. 9(a-f): Effects of ligustrazine on ultrasound imaging parameters, (a) ACT, (b) a2, (c) a3, (d) ISI, (e) AUC and (f) BF
*,**Suggested a great difference with p<0.05 and p<0.01, respectively

Effects of ligustrazine on ultrasound imaging parameters: The impacts of ligustrazine on ultrasound imaging parameters were illustrated in Fig. 9. The ACT and ISI values in the ligustrazine group were lower ($p<0.05$) (Fig. 9a, d), the a2 value was higher ($p<0.05$) (Fig. 9b) and the a3 (Fig. 9c), AUC (Fig. 9e) and BF (Fig. 9f) values were extremely higher ($p<0.01$) in contrast to those in the Ctrl group.

DISCUSSION

The extraction conditions directly influence the extraction efficiency of the target compounds. In this study, the effects of various parameters including ethanol concentration, ethanol volume, number of extractions, extraction time and extraction temperature on the extraction efficiency of ligustrazine were compared. The results revealed that the highest concentration of ligustrazine was obtained when using 75% ethanol concentration. This indicates that within a certain range, the ethanol solution concentration promotes the extraction of ligustrazine[21]. When the ethanol concentration was 75%, the extraction efficiency of ligustrazine was optimal. The research findings indicated that the highest concentration of ligustrazine was achieved when using 100 mL of ethanol. This indicates that initially, increasing the ethanol volume improved the extraction efficiency of ligustrazine, resulting in an increased concentration of extracted ligustrazine[22]. When the ethanol volume exceeded 100 mL, the concentration of ligustrazine did not increase further. This may be because the active components in the ethanol solution reached saturation and could not extract more ligustrazine. Subsequently, this study revealed that conducting the extraction process three times yielded a higher concentration of ligustrazine. Moreover, the extraction duration needed to exceed 180 min, with the optimal extraction temperature identified as 60°C. This may be due to degradation or other reactions of ligustrazine occurring under high-temperature conditions, resulting in a decrease in the extraction efficiency[23,24]. At low temperatures, the solubility of ligustrazine is relatively low and at high temperatures, the extraction efficiency of ligustrazine decreases. Additionally, ligustrazine is prone to sublimation, so it is recommended to control the extraction temperature around 60°C during the reflux process. Subsequently, this study examined the stability of extracted ligustrazine, revealing that its concentration gradually decreased with prolonged storage time under room temperature and 4°C conditions. Although the decrease in concentration was slower when stored at 4°C, there was no significant difference observed. This suggests that ligustrazine exhibits relatively better stability at low temperatures, with slower rates of degradation or other reactions, indicating temperature is a critical factor influencing ligustrazine stability[25]. Ligustrazine, being a natural product, may undergo changes in its chemical properties and activity under different temperature conditions[26]. Under low-temperature conditions, ligustrazine may crystallize or solidify[27], while under high temperatures, it is prone to volatilization and degradation[28]. Therefore, temperature control within an appropriate range during the storage and utilization of ligustrazine is essential to ensure the stability of its properties and effects.

The LSCC is a disease characterized by abnormal proliferation of squamous cells in the larynx and pharynx, representing the most common malignant epithelial tumor in the upper respiratory tract and closely associated with factors such as smoking and alcohol consumption. Ligustrazine, on the other hand, exhibits a wide range of pharmacological effects, including vasodilation, increased arterial blood flow and inhibition of platelet aggregation. Additionally, ligustrazine has been shown to inhibit tumor cell proliferation and metastasis while promoting tumor cell apoptosis, suggesting its potential as a therapeutic agent for cancer treatment. The results demonstrated that ligustrazine significantly inhibited the proliferation of LSCC cells in a concentration-dependent manner, indicating its potential as a promising candidate for the treatment of LSCC. Ligustrazine inhibits cancer cell proliferation through various mechanisms, including the inhibition of cell cycle progression, induction of apoptosis, suppression of AKT/mTOR signaling pathway activation and anti-angiogenic effects[29,30]. Research findings suggested that ligustrazine may inhibit cancer cell proliferation by suppressing the activation of the AKT/mTOR signaling pathway[31]. Treatment with ligustrazine can reduce the phosphorylation status of the AKT/mTOR signaling pathway and inhibit the expression and activity of mTOR protein, thereby suppressing cell proliferation[32]. Therefore, this study further investigated the effects of ligustrazine on the status of the AKT/mTOR signaling pathway in LSCC cells. The AKT/mTOR (protein kinase B-acetylation activated transcription factor/mammalian target of rapamycin) SPW is associated with the proliferation ability of LSCC cells[33]. This SPW importantly regulates the cells and regulates cell growth, proliferation, survival and metabolism[34,35]. Abnormal activation of the AKT/mTOR SPW is correlated with enhanced cell proliferation ability in LSCC[36]. The AKT is a crucial signaling protein kinase that can activate the mTOR SPW by

phosphorylating mTOR. Activated AKT/mTOR SPW can be beneficial for the proliferation and growth of LSCC cells and inhibit their apoptosis (necrosis)[37]. Therefore, inhibiting the AKT/mTOR SPW could be a potential strategy for treating LSCC. By using AKT/mTOR SPW inhibitors or other drugs, it is possible to interfere with the activation of this pathway, inhibit cell proliferation and potentially suppress the development and progression of LSCC[38]. The results demonstrated that ligustrazine significantly inhibited the phosphorylation of AKT and mTOR proteins in LSCC cells, exhibiting a concentration-dependent characteristic. The decrease in phosphorylation status may reflect the inhibition of the AKT/mTOR signaling pathway, indicating that ligustrazine may affect the biological activity of LSCC cells by inhibiting the phosphorylation of AKT and mTOR proteins.

To further understand the therapeutic effects of ligustrazine on LSCC, this study established a nude mouse model with LSCC xenografts. The results revealed that treatment with ligustrazine led to a significant reduction in tumor weight and volume in the LSCC xenograft nude mouse model. Additionally, an increase in body weight of the nude mice was observed, accompanied by a notable decrease in tumor volume. These findings suggest that ligustrazine may inhibit the growth of LSCC xenografts in nude mice, demonstrating the potential for suppressing tumor growth and metastasis, thereby implying its anti-tumor efficacy. Moreover, ligustrazine positively impacted the overall health status of the nude mice, reducing the decrease in net weight induced by tumor burden. Ligustrazine was found to enhance immune function and antioxidant capacity, mitigating tumor-induced damage in nude mice and thereby improving their overall health condition, manifested by an increase in net weight. Subsequently, this study utilized contrast-enhanced ultrasound imaging technology to evaluate the effects of ligustrazine treatment on the hemodynamics of LSCC xenograft nude mouse models. The results indicated a decrease in ACT, ISI, AUC and BF indices, while the a2 and a3 indices increased. This suggested that ligustrazine may influence the hemodynamic behavior of LSCC xenograft nude mouse models by inhibiting vasodilation, reducing blood flow velocity and improving blood circulation, thereby promoting hemodynamic responses and enhancing blood perfusion conditions. Ligustrazine possesses pharmacological effects such as anti-inflammatory, anticoagulant and vasodilatory properties. These effects may result in lower values for ACT and ISI in the ligustrazine group, possibly associated with its inhibition of vasodilation, suppression of increased blood flow velocity or improvement of blood circulation. These morphological changes may represent one of the potential mechanisms underlying the effects of ligustrazine on hemodynamic parameters.

CONCLUSION

In this work, a natural extract, ligustrazine, was isolated from the Chinese medicinal herb *Ligusticum wallichii* using ethanol reflux, vacuum concentration and macroporous resin adsorption separation methods. The effects of ethanol concentration, ethanol volume, extraction cycles, time and temperature on ligustrazine concentration were analyzed. Additionally, the storage stability of ligustrazine was assessed. Inhibition of ligustrazine on the proliferation of LSCC cells and AKT/mTOR SPW-related proteins were determined. In addition, the impacts of ligustrazine on ultrasound imaging were also analyzed. The results revealed that the highest extraction efficiency of ligustrazine was achieved using a 75% ethanol solution with a volume of 100 mL, subjected to 3 extraction cycles, at a stable extraction temperature of 60°C for 180 min. Furthermore, ligustrazine exhibited good storage stability at 4°C. Ligustrazine inhibited the proliferation of LSCC cells, which may be attributed to its ability to suppress the phosphorylation of AKT and mTOR. Moreover, based on the performance of contrast-enhanced ultrasound imaging, ligustrazine promoted the dynamic response of blood flow and influenced its dynamic behavior, providing new options and insights for LSCC treatment.

SIGNIFICANCE STATEMENT

The objective of this study was to evaluate the inhibitory effect of ligustrazine on the proliferation of laryngeal squamous cell carcinoma cells and its influence on contrast-enhanced ultrasound imaging, thereby investigating its potential anti-tumor efficacy and impact on contrast-enhanced ultrasound imaging parameters. The results demonstrated that ligustrazine significantly suppressed the proliferation of LSCC cells, exerting its effects through the modulation of the AKT/mTOR signaling pathway. Additionally, ligustrazine affected hemodynamic responses, improving the performance of contrast-enhanced ultrasound imaging. These findings are of paramount significance in elucidating the mechanistic role of ligustrazine in anti-tumor therapy. Future research endeavors may further explore the clinical application potential of ligustrazine in the treatment of LSCC and delve into its utility in contrast-enhanced ultrasound imaging.

REFERENCES

1. Song, L., S. Zhang, S. Yu, F. Ma and B. Wang *et al*., 2020. Cellular heterogeneity landscape in laryngeal squamous cell carcinoma. Int. J. Cancer, 147: 2879-2890.
2. Tsiambas, E., N. Mastronikolis, P.P. Fotiades, E. Kyrodimos and A. Chrysovergis *et al*., 2020. c-Jun/c-Fos complex in laryngeal squamous cell carcinoma. JBUON, 25: 618-620.
3. Yan, L., X. Song, G. Yang, L. Zou, Y. Zhu and X. Wang, 2022. Identification and validation of immune infiltration phenotypes in laryngeal squamous cell carcinoma by integrative multi-omics analysis. Front. Immunol., Vol. 13. 10.3389/fimmu.2022.843467.
4. Ma, J., X. Hu, B. Dai, Q. Wang and H. Wang, 2021. Bioinformatics analysis of laryngeal squamous cell carcinoma: Seeking key candidate genes and pathways. PeerJ, Vol. 9. 10.7717/peerj.11259.
5. Li, G.S., L.J. Yang, G. Chen, S.N. Huang and Y.Y. Fang *et al*., 2022. Laryngeal squamous cell carcinoma: Clinical significance and potential mechanism of cell division cycle 45. Cancer Biother. Radiopharm., 37: 300-312.
6. Mao, Z., L. Tian, J. Liu, Q. Wu and N. Wang *et al*., 2022. Ligustilide ameliorates hippocampal neuronal injury after cerebral ischemia reperfusion through activating PINK1/Parkin-dependent mitophagy. Phytomedicine, Vol. 101. 10.1016/j.phymed.2022.154111.
7. Wu, Q., J. Liu, Z. Mao, L. Tian and N. Wang *et al*., 2022. Ligustilide attenuates ischemic stroke injury by promoting Drp1-mediated mitochondrial fission via activation of AMPK. Phytomedicine, Vol. 95. 10.1016/j.phymed.2021.153884
8. Hsu, R.J., K.Y. Peng, W.L. Hsu, Y.T. Chen and D.W. Liu, 2022. Z-Ligustilide induces c-Myc-dependent apoptosis *via* activation of ER-stress signaling in hypoxic oral cancer cells. Front. Oncol., Vol. 12. 10.3389/fonc.2022.824043.
9. Ma, J., J. Mei, J. Lu, Y. Wang and M. Hu *et al*., 2020. Ligustilide promotes apoptosis of cancer-associated fibroblasts via the TLR4 pathways. Food Chem. Toxicol., Vol. 135. 10.1016/j.fct.2019.110991.
10. Zhang, B., D. Wu, L. Hu, X. Cha and Y. Liu *et al*., 2022. Ligustilide inhibits the proliferation of human osteoblastoma MG63 cells through the TLR4-ERK pathway. Life Sci., Vol. 288. 10.1016/j.lfs.2020.118993.
11. Jiang, X., W. Zhao, F. Zhu, H. Wu and X. Ding *et al*., 2021. Ligustilide inhibits the proliferation of non-small cell lung cancer *via* glycolytic metabolism. Toxicol. Appl. Pharmacol., Vol. 410. 10.1016/j.taap.2020.115336.
12. Peng, D., H.Z. Qiao, H.Y. Tan, Y.X. Wang, and D. Luo *et al*., 2022. Ligustilide ameliorates cognitive impairment via AMPK/SIRT1 pathway in vascular dementia rat. Metab. Brain Dis., 37: 1401-1414.
13. Ma, J., Y. Xu, Q. Zheng, Y. Wang and M. Hu *et al*., 2019. Ligustilide inhibits the activation of cancer-associated fibroblasts. Life Sci., 218: 58-64.
14. Ma, J., X. Chen, Y. Chen, N. Tao and Z. Qin, 2022. Ligustilide inhibits tumor angiogenesis by downregulating VEGFA secretion from cancer-associated fibroblasts in prostate cancer via TLR4. Cancers, Vol. 14. 10.3390/cancers14102406.
15. Zhu, W.L., J.Y. Zheng, W.W. Cai, Z. Dai and B.Y. Li *et al*., 2020. Ligustilide improves aging-induced memory deficit by regulating mitochondrial related inflammation in SAMP8 mice. Aging, 12: 3175-3189.
16. Ren, C., N. Li, C. Gao, W. Zhang and Y. Yang *et al*., 2020. Ligustilide provides neuroprotection by promoting angiogenesis after cerebral ischemia. Neurol. Res., 42: 683-692.
17. Yang, J. and Z. Xing, 2021. Ligustilide counteracts carcinogenesis and hepatocellular carcinoma cell-evoked macrophage M2 polarization by regulating yes-associated protein-mediated interleukin-6 secretion. Exp. Biol. Med., 246: 1928-1937.
18. Ahn, D., J.H. Kwak, G.J. Lee and J.H. Sohn, 2022. Ultrasonography for masses of the pharynx and larynx and assessment of laryngeal squamous cell carcinoma. Auris Nasus Larynx, 49: 868-874.
19. Liu, J.L., S.L. Zheng, Q.J. Fan, J.C. Yuan, S.M. Yang and F.L. Kong, 2014. Optimization of high-pressure ultrasonic-assisted simultaneous extraction of six major constituents from ligusticum chuanxiong rhizome using response surface methodology. Molecules, 19: 1887-1911.
20. McCarville, M.B., C.J. Streck, P.V. Dickson, C.S. Li, A.C. Nathwani and A.M. Davidoff, 2006. Angiogenesis inhibitors in a murine neuroblastoma model: Quantitative assessment of intratumoral blood flow with contrast-enhanced gray-scale US. Radiology, 240: 73-81.
21. Wei, W.L., R. Zeng, C.M. Gu, Y. Qu and L.F. Huang, 2016. *Angelica sinensis* in China-A review of botanical profile, ethnopharmacology, phytochemistry and chemical analysis. J. Ethnopharmacol., 190: 116-141.
22. Chen, H., Y. Zhao, G. Qin, Y. Bi and G. Yue *et al*., 2022. Antifungal effects and active components of *Ligusticum chuanxiong*. Molecules, Vol. 27. 10.3390/molecules27144589.
23. Hoshino, Y., Wahyudiono, S. Machmudah, S. Hirayama, H. Kanda, M. Hoshino and M. Goto, 2022. Extraction of functional components from freeze-dried *Angelica furcijuga* leaves using supercritical carbon dioxide. ACS Omega, 7: 5104-5111.
24. Chen, Q.C., J. Lee, W. Jin, U. Youn and H. Kim *et al*., 2007. Cytotoxic constituents from *Angelicae sinensis* Radix. Arch. Pharm. Res., 30: 565-569.
25. Schinkovitz, A., S.M. Pro, M. Main, S.N. Chen, B.U. Jaki, D.C. Lankin and G.F. Pauli, 2008. Dynamic nature of the ligustilide complex. J. Nat. Prod., 71: 1604-1611.

26. Luo, Z., A. Zeng, Y. Chen, S. He and S. He *et al*., 2021. Ligustilide inhibited angiotensin II induced A7r5 cell autophagy via Akt/mTOR signaling pathway. Eur. J. Pharmacol, Vol. 905. 10.1016/j.ejphar.2021.174184.
27. Yin, J., C. Wang, A. Mody, L. Bao, S.H. Hung, S.A. Svoronos and Y. Tseng, 2013. The effect of Z-ligustilide on the mobility of human glioblastoma T98G cells. PLoS ONE, Vol. 8. 10.1371/journal.pone.0066598.
28. Chen, T., X. Zhu, Q. Chen, M. Ge, X. Jia, X. Wang and C. Ge, 2015. Interaction between Z-ligustilide from *Radix Angelica sinensis* and human serum albumin. Food Chem., 186: 292-297.
29. Li, X., D. Wu, Z. Hu, J. Xuan and X. Ding *et al*., 2018. The protective effect of ligustilide in osteoarthritis: An *in vitro* and *in vivo* study. Cell. Physiol. Biochem., 48: 2583-2595.
30. Ye, Y.T., W. Zhong, P. Sun, D. Wang, C. Wang, L.M. Hu and J.Q. Qian, 2017. Apoptosis induced by the methanol extract of *Salvia miltiorrhiza Bunge* in non-small cell lung cancer through PTEN-mediated inhibition of PI3K/Akt pathway. J. Ethnopharmacol., 200: 107-116.
31. Wu, Q., Z. Mao, J. Liu, J. Huang and N. Wang, 2020. Ligustilide attenuates ischemia reperfusion-induced hippocampal neuronal apoptosis via activating the PI3K/Akt pathway. Front. Pharmacol., Vol. 11. 10.3389/fphar.2020.00979.
32. Kuang, X., H.J. Zhou, A.H. Thorne, X.N. Chen, L.J. Li and J.R. Du, 2017. Neuroprotective effect of ligustilide through induction of α-secretase processing of both app and klotho in a mouse model of Alzheimer's disease. Front. Aging Neurosci., Vol. 9. 10.3389/fnagi.2017.00353.
33. Gao, W., H. Guo, M. Niu, X. Zheng and Y. Zhang *et al*., 2020. *circPARD3* drives malignant progression and chemoresistance of laryngeal squamous cell carcinoma by inhibiting autophagy through the PRKCI-Akt-mTOR pathway. Mol. Cancer, Vol. 19. 10.1186/s12943-020-01279-2.
34. Wang, J., L. Lan, B. Ma, G. Ren and C. Yin, 2022. KRT17accelerates cell proliferative and invasive potential of laryngeal squamous cell carcinoma (LSCC) through regulating AKT/mTOR and Wnt/β-catenin pathways. Evidence-Based Complementary Altern. Med., Vol. 2022. 10.1155/2022/6176043.
35. Zhao, R., L. Tian, B. Zhao, Y. Sun and J. Cao *et al*., 2020. FADS1 promotes the progression of laryngeal squamous cell carcinoma through activating AKT/mTOR signaling. Cell Death Dis., Vol. 11. 10.1038/s41419-020-2457-5.
36. Zhu, X. and R. Zhu, 2018. Curcumin suppresses the progression of laryngeal squamous cell carcinoma through the upregulation of miR-145 and inhibition of the PI3K/Akt/mTOR pathway. OncoTargets Ther., 11: 3521-3531.
37. Huang, H.Y., K.N. Li, H.C. Lau, C.Y. Hsueh, N. Cong and M. Zhang, 2022. Dual inhibition of autophagy and PI3K/mTOR pathway as a potential therapeutic strategy against laryngeal squamous cell carcinoma. Transl. Cancer Res., 11: 1076-1088.
38. Yu, L., H. Cao, J.W. Yang, W.X. Meng and C. Yang *et al*., 2023. HDAC5-mediated PRAME regulates the proliferation, migration, invasion, and EMT of laryngeal squamous cell carcinoma via the PI3K/AKT/mTOR signaling pathway. Open Med., Vol. 18. 10.1515/med-2023-0665.